

Intrinsic GTPase Activity of K-RAS Monitored by Native Mass Spectrometry

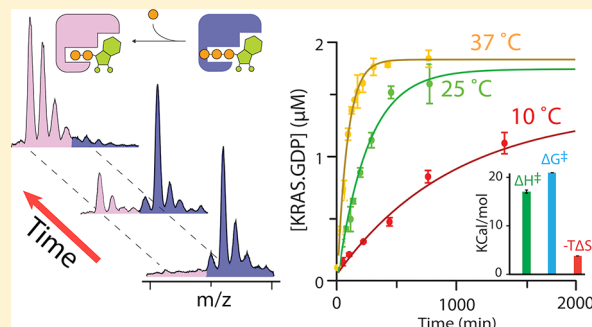
Zahra Moghadamchargari,[†] Jamison Huddleston,[†] Mehdi Shirzadeh,[†] Xueyun Zheng,[†] David E. Clemmer,[‡] Frank M. Rauschel,[†] David H. Russell,[†] and Arthur Laganowsky^{*,†,‡}

[†]Department of Chemistry, Texas A&M University, College Station, Texas 77843, United States

[‡]Department of Chemistry, Indiana University, Bloomington, Indiana, 47405, United States

S Supporting Information

ABSTRACT: Mutations in RAS are associated with many different cancers and have been a therapeutic target for more than three decades. RAS cycles from an active to inactive state by both intrinsic and GTPase-activating protein (GAP)-stimulated hydrolysis. The activated enzyme interacts with downstream effectors, leading to tumor proliferation. Mutations in RAS associated with cancer are insensitive to GAP, and the rate of inactivation is limited to their intrinsic hydrolysis rate. Here, we use high-resolution native mass spectrometry (MS) to determine the kinetics and transition state thermodynamics of intrinsic hydrolysis for K-RAS and its oncogenic mutants. MS data reveal heterogeneity where both 2'-deoxy and 2'-hydroxy forms of GDP (guanosine diphosphate) and GTP (guanosine triphosphate) are bound to the recombinant enzyme. Intrinsic GTPase activity is directly monitored by the loss in mass of K-RAS bound to GTP, which corresponds to the release of phosphate. The rates determined from MS are in direct agreement with those measured using an established solution-based assay. Our results show that the transition state thermodynamics for the intrinsic GTPase activity of K-RAS is both enthalpically and entropically unfavorable. The oncogenic mutants G12C, Q61H, and G13D unexpectedly exhibit a 2'-deoxy GTP intrinsic hydrolysis rate higher than that for GTP.



RAS proteins regulate diverse cellular processes, including cell proliferation, apoptosis, differentiation, migration, and cell growth.^{1–6} RAS proteins function as a molecular switch cycling between inactive guanosine diphosphate (GDP)- and active guanosine triphosphate (GTP)-bound states.^{7–10} Conformational changes in three main regions of RAS are associated with the exchange of bound GDP for GTP: switch I (residues 30–38), switch II (residues 59–76), and P-loop (residues 10–17).¹¹ In the active state, RAS binds and activates downstream effectors (Raf kinase, PI3K, and Ral guanine nucleotide dissociation stimulator).¹¹ RAS proteins possess low intrinsic GTP hydrolysis and guanidine nucleotide exchange rates.^{12,13} These attributes are regulated by guanine nucleotide exchange factors (GEFs), which accelerate the exchange of GDP for GTP, and GTPase-activating proteins (GAPs), which stimulate the hydrolysis of GTP leading to deactivation of the active state.¹⁴

The first mutated genes in human cancers were discovered nearly four decades ago that mapped to activating mutations in RAS genes.^{15,16} To date, the three RAS proteins (H-RAS, K-RAS, and N-RAS) have a high overall level of sequence identity and are the most commonly mutated of all discovered oncogenes with 30% of human cancers containing RAS mutations.^{13,17,18} Nearly all oncogenic RAS genes contain mutations that map to residues G12, G13, and Q61, which

often impairs the intrinsic and GAP-stimulated GTP hydrolysis leading to unregulated cell signaling and tumor growth.^{13,19–22} More specifically, K-RAS is the most frequently mutated isoform that has a high frequency in pancreatic cancer (70–90%), colon cancer (30–50%), and lung cancer (20–30%).^{23–25} K-RAS oncogenic mutants exhibit differences in the biological behavior of tumors, and understanding the intrinsic biochemical and structural properties of oncogenic mutants can potentially accelerate the development of therapeutics.^{26–28}

The kinetics of GTP hydrolysis for RAS proteins has been extensively studied by an arsenal of biochemical and biophysical methods, such as nuclear magnetic resonance (NMR), Fourier transform infrared spectroscopy (FTIR), radiolabeled substrates, and spectroscopic assays wherein the amount of phosphate released by enzymatic hydrolysis is monitored.^{20,29–31} RAS proteins can switch to an inactive state either through intrinsic hydrolysis or by interacting with GAPs that accelerate the hydrolysis rate by 10⁵-fold.³² Previous studies have shown RAS has a slow intrinsic hydrolysis rate and oncogenic mutations display an even slower rate of GTP

Received: June 19, 2019

Revised: July 11, 2019

Published: July 15, 2019

hydrolysis that essentially locks RAS in an active state. The energetics of intrinsic GTP hydrolysis determined for H-RAS suggests that the enthalpic effect is the dominant barrier of the transition state.³³

Native mass spectrometry (MS) is an emerging biophysical technique for studying protein structure and function.^{34,35} In native MS, protein complexes in a volatile, nondenaturing solution (typically ammonium acetate) are ionized using nano-electrospray ionization^{36,37} and the instrument is tuned to preserve protein structure and noncovalent interactions in the mass spectrometer.^{38–40} This unique ability has enabled the analysis of direct ligand binding, protein dynamics and topology, and subunit stoichiometry and measurement of thermodynamics and binding affinities.^{41–45} More recently, high-resolution native mass spectrometry has been used to characterize the binding of small molecules such as drugs, nucleotides, lipids, metals, and small enzyme cofactors.^{42,46,47} Ion mobility (IM) is a gas phase electrophoretic separation of molecules based on the size and shape of ions, and when it is combined with MS, it can provide structural information by measuring the rotationally averaged collision cross section (CCS). Native IM-MS can monitor direct molecular interactions of molecules with protein complexes and also provide unparalleled insight into the purity of protein samples.^{37,48}

Here, we use high-resolution native MS to directly measure the kinetics and energetics of intrinsic GTP hydrolysis of K-RAS and oncogenic mutants: G12C, G13D, and Q61H. The “as-isolated” mass spectra of K-RAS and mutants reveal the heterogeneity of the enzyme where both 2'-deoxy and 2'-hydroxy forms of GDP and GTP are bound. Hydrolysis of GTP to GDP and inorganic phosphate was monitored directly by the decrease in m/z of the intact ion from K-RAS-GTP to K-RAS-GDP. The intrinsic hydrolysis rates determined by native MS are in direct agreement with a spectroscopic assay that measures the concentration of inorganic phosphate. The hydrolysis rate of 2'-deoxy GTP (dGTP) was also monitored using mass spectrometry, and results show that three oncogenic mutants, Q61H, G13D, and G12C, have a dGTP hydrolysis rate that is higher than that for GTP. The energetics of hydrolysis for K-RAS and oncogenic mutants reveal the transition state is both enthalpically and entropically unfavorable, with the enthalpic term being the largest barrier in the hydrolysis of GTP. Taken together, our results emphasize the utility of native high-resolution MS to study the kinetic and thermodynamic properties of K-RAS, including other GTPases, and uncover heterogeneity of nucleotides bound to K-RAS that might be unrecognized using other biophysical techniques.

MATERIALS AND METHODS

Protein Expression and Purification. The K-RAS4B (residues 1–170, UniProt entry P01116-2) plasmid for expression in *Escherichia coli* was a kind gift from K. D. Westover (University of Texas Southwestern Medical Center, Dallas, TX). The K-RAS4B (here termed K-RAS) construct included an N-terminal TEV protease cleavable His₆ tag. All mutations were generated using the Q5 site-directed mutagenesis kit (New England Biolabs) following the manufacturer's protocol. Plasmids were transformed into Lemo21- (DE3) *E. coli* (New England Biolabs) for protein expression. Several colonies were grown overnight at 37 °C in Luria broth (LB) supplemented with 50 μg/mL kanamycin. One liter of

LB was inoculated with an overnight culture and grown at 37 °C to an OD (600 nm) of 0.8. Protein expression was induced by addition of isopropyl β-D-1-thiogalactopyranoside (IPTG) to a final concentration of 500 μM, and cells were grown overnight at 18 °C. Cells were harvested by centrifugation at 5000g, and cell pellets stored at –80 °C. Cell pellets were thawed at room temperature and resuspended in resuspension buffer [500 mM sodium chloride and 20 mM 2-amino-2-(hydroxymethyl)-1,3-propanediol (TRIS) (pH 7.4) at room temperature] supplemented with a complete protease inhibitor tablet (Roche) and 5 mM β-mercaptoethanol (β-ME). The cell suspension was passed three times through a microfluidizer (Microfluidics M-110P) at 20000 psi. The lysate was clarified by centrifugation at 30000g for 30 min, and imidazole was added to a final concentration of 20 mM. The lysate was filtered using a 0.45 μm syringe filter prior to being loaded onto a 5 mL HisTrap HP column (GE Healthcare) pre-equilibrated in buffer A [300 mM NaCl, 20 mM imidazole, 5 mM β-ME, 20% glycerol, and 20 mM TRIS (pH 7.4) at room temperature]. The protein was eluted with buffer A containing 500 mM imidazole. The peak fractions were pooled and desalted using a HiPrep 26/10 desalting column (GE Healthcare) equilibrated in buffer A. The desalted protein was then digested with TEV protease at 4 °C overnight to remove the N-terminal purification tag. The sample was passed over a 5 mL HisTrap HP column, and the flow-through containing tag-less protein was collected. The sample was further diluted (six times), loaded onto a 5 mL HiTrap Q HP column (GE Healthcare) equilibrated with buffer B [50 mM sodium chloride and 20 mM TRIS (pH 8) at room temperature], and eluted with a linear gradient to 100% buffer C [1 M sodium chloride and 20 mM TRIS (pH 8) at room temperature] over 5 column volumes. The peak fractions containing protein were pooled, concentrated, and injected onto a Highload 16/600 Superdex 75 pg column (GE Healthcare) equilibrated in buffer D [150 mM sodium chloride, 5 mM β-ME, 20% glycerol, and 20 mM 4-(2-hydroxyethyl)-1-piperazineethanesulfonic acid (HEPES) (adjusted to pH 7.4)]. Peak fractions containing protein were pooled, concentrated using a centrifugal concentrator [Millipore, 10K molecular weight cutoff (MWCO)], flash-frozen with liquid nitrogen, and stored at –80 °C.

Determination of the Protein Concentration. The protein concentration was determined using an ultraviolet–visible (UV–vis) spectrometer (Biospectrometer eppendorf) at 280 nm using an extinction coefficient of 11920 M^{–1} cm^{–1}.

Nucleotide Exchange Assay. K-RAS and its oncogenic mutants at a concentration of 100 μM were incubated in buffer D supplemented with 10 mM ethylenediaminetetraacetic acid (EDTA) and either 2 mM GTP (guanosine 5'-triphosphate, Sigma-Aldrich) or dGTP (2'-deoxyguanosine 5'-triphosphate, Sigma-Aldrich) for 2 h at 4 °C. The nucleotide exchange reaction mixture was then supplemented with 10 mM magnesium chloride and incubated for an additional 1 h at 4 °C. Excess nucleotide was removed using a centrifugal buffer exchange device (Micro Bio-Spin 6 Column, Bio-Rad). To fully exchange GDP with GTP, this procedure was repeated once more. The nucleotide-exchanged sample was then supplemented with either GTP or dGTP at a final concentration of 2 mM, added to a Slide-A-Lyzer MINI device (2000 Da MWCO, Thermo), and dialyzed against 200 mM ammonium acetate overnight at 4 °C.

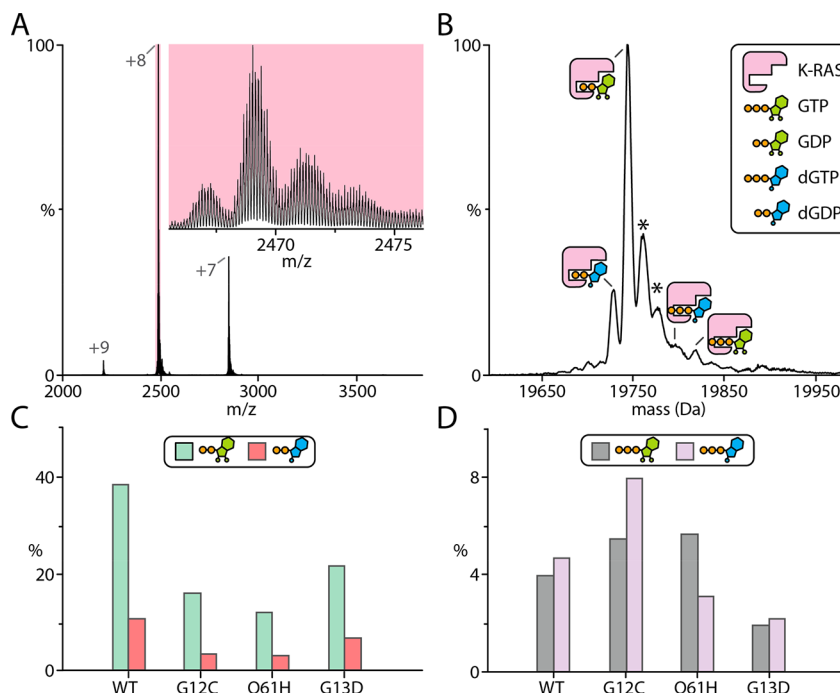


Figure 1. Native mass spectrometry reveals heterogeneity of “as-isolated” K-RAS and its mutants. (A) Native mass spectrum of 2 μM K-RAS in 200 mM ammonium acetate (pH 7.4). The inset is an expansion of the isotopically resolved 8+ charge state of K-RAS bound to GDP. (B) Deconvolution of the mass spectrum shown in panel A using UniDec.⁵⁰ The different nucleotide-bound states of K-RAS are labeled. Asterisks denote sodium- and/or magnesium-bound adducts. Mole fractions of K-RAS and its mutants bound to the 2'-deoxy and 2'-hydroxy forms of (C) GDP and (D) GTP.

Native Mass Spectrometry. The protein loaded with either GTP or dGTP was buffer exchanged using a Micro Bio-Spin 6 device into 200 mM ammonium acetate (pH 7.4) (pH adjusted with ammonium hydroxide) and incubated at 25 °C. To monitor hydrolysis, samples were loaded into pulled borosilicate glass capillaries prepared in house⁴⁹ and electrosprayed with a voltage applied through a platinum wire inserted directly into the solution. Samples were introduced into Thermo Exactive Plus with an extended mass range Orbitrap mass spectrometer. The mole fractions of GDP-bound K-RAS ($F_{K-RAS-GDP}$) at different time points were deconvoluted using Unidec⁵⁰ and calculated as follows:

$$F_{K-RAS-GDP} = \frac{\sum_{i=0}^3 K-RAS-GDP \cdot A_i}{\sum_{i=0}^3 K-RAS-GDP \cdot A_i + \sum_{i=0}^3 K-RAS-GTP \cdot A_i}$$

where i represents the number of adducts (A) bound to K-RAS. The mole fraction was converted to concentration:

$$[K-RAS-GDP]_{total} = P_{total} F_{K-RAS-GDP}$$

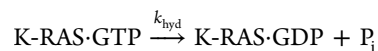
and P_{total} is the total concentration of the enzyme. The mole fraction and concentration of K-RAS-bound GTP were calculated in a similar fashion. To obtain thermodynamic parameters for GTP hydrolysis, loaded proteins were incubated at four different temperatures: 10, 25, 30, and 37 °C. Instrument parameters (Table S1) were tuned to minimize gas phase activation and to preserve noncovalent interactions.

Native Ion Mobility Mass Spectrometry. K-RAS and its mutants were fully loaded with GTP and analyzed using an Agilent 6560 ion mobility Q-TOF mass spectrometer (Agilent Technologies, Santa Clara, CA).⁵¹ For native ion mobility mass spectrometry (IM-MS) measurements, ions were generated from a nanoelectrospray ionization source. Ions

were then pulsed into the drift tube filled with ~3.95 Torr of nitrogen gas, where they traveled under the influence of a weak electric field (5 V cm⁻¹ Torr⁻¹). Ions exiting the drift tube were refocused by a rear ion funnel prior to QTOF MS detection, and their arrival times (t_A) recorded. CCS values were determined from first principles with data acquired at different drift voltages.⁵² Instrumental settings are listed in Tables S2 and S3. The Agilent IM-MS Browser software was utilized to extract arrival time distributions (ATDs), IMS data processing, and all stepped field CCS calculations.

Malachite Green Assay. The intrinsic hydrolysis of K-RAS was monitored using a malachite green assay.⁵³ In brief, malachite green reagent (1 mg/mL malachite green, 100 mg/mL ammonium molybdate, and 0.01% Triton X-100 in 50 mL of 1 M hydrochloric acid) was prepared as described previously.⁵⁴ A standard curve was generated by serial dilutions of 1 mM dipotassium phosphate. The concentration of inorganic phosphate released during hydrolysis was determined at different time intervals for K-RAS loaded with GTP. For each time point, 30 μL of malachite green reagent was added to 10 μL of 10 μM K-RAS and the mixture incubated for 15 min. The absorbance was measured at 650 nm using a Synergy (MX) plate reader. All measurements were done in triplicate, and solutions were made using OmniTrace Ultra water (Sigma-Aldrich) to minimize background phosphate.

Analysis of Intrinsic GTPase Data. Kintek Explorer (version 7.6) was used to globally fit the kinetic data to a first-order rate constant as follows:



And the integrated form:

$$[K-RAS \cdot GTP] = [K-RAS \cdot GTP]_0 e^{-k_{hyd} t}$$

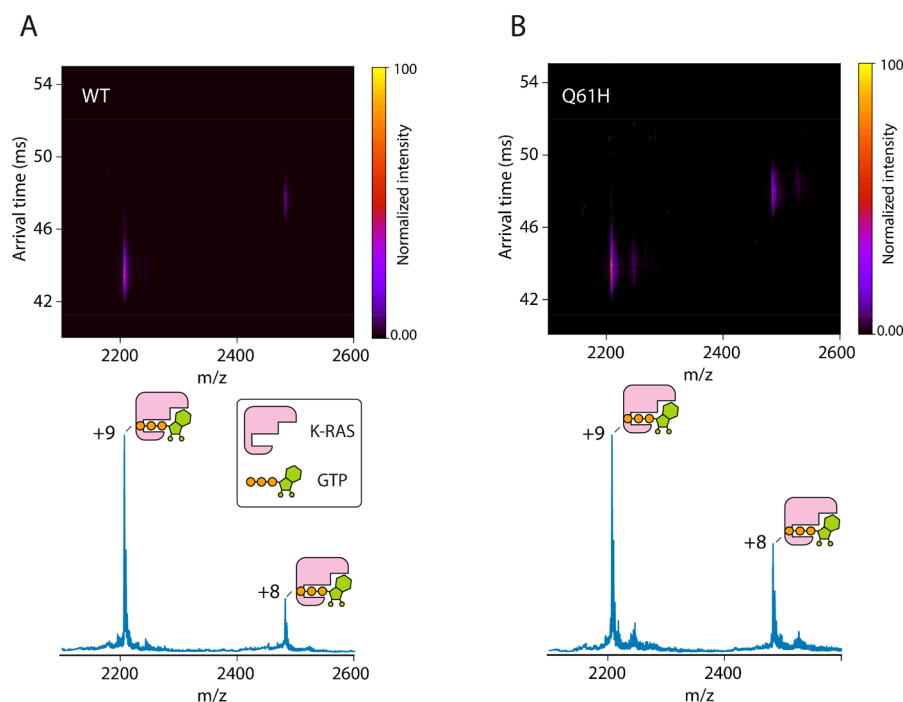


Figure 2. Ion mobility mass spectra of K-RAS and its Q61H mutant. (A) K-RAS and (B) K-RAS^{Q61H} loaded with GTP. The mass spectra are shown at the bottom.

The rate of the reverse reaction was assumed to be negligible. To obtain the energetics of intrinsic hydrolysis, the temperature dependence of the rate constants was analyzed using the Eyring⁵⁵ equation:

$$k_{\text{hyd}} = \frac{k_{\text{B}}T}{h} e^{-\Delta H^{\ddagger}/RT + \Delta S^{\ddagger}/R}$$

where k_{hyd} is the intrinsic hydrolysis rate constant, h is Planck's constant, k_{B} is Boltzmann's constant, R is the gas constant, ΔH^{\ddagger} is the enthalpy of activation, and ΔS^{\ddagger} is the entropy of activation. To calculate ΔH^{\ddagger} and ΔS^{\ddagger} , the linearized form of the Eyring equation was used:

$$\ln \frac{k_{\text{hyd}}}{T} = \frac{-\Delta H^{\ddagger}}{RT} + \frac{\Delta S^{\ddagger}}{R} + \ln \frac{k_{\text{B}}}{T}$$

The natural log of k_{hyd}/T was plotted as a function of $1/T$. ΔH^{\ddagger} and ΔS^{\ddagger} parameters were calculated from slope and intercept of this plot as follows:

$$\Delta H^{\ddagger} = -\text{slope} \times R$$

$$\Delta S^{\ddagger} = \left(\text{intercept} - \ln \frac{k_{\text{B}}}{T} \right) R$$

RESULTS

Heterogeneity of “As-Isolated” K-RAS and Its Oncogenic Mutants. Previous work suggested that native MS can accurately reflect the solution binding properties of small molecules with proteins.^{41–45} Therefore, we recorded native mass spectra of purified protein samples on an Orbitrap mass spectrometer tuned to preserve noncovalent interactions (Figure 1A).⁴⁶ After deconvolution of native mass spectra,⁵⁰ a number of molecular species were observed for the “as-isolated” proteins (Figure 1B and Table S4). For K-RAS, the most intense signal has a molecular weight in agreement with

that of K-RAS bound to GDP (guanosine 5'-diphosphate), a hydrolysis product (Figure 1B).

Interestingly, a mass that is 16 Da lighter is also measured, which corresponds to K-RAS bound to 2'-deoxyguanosine 5'-diphosphate (dGDP), although at lower abundances, a signal is present for the molecular weights of K-RAS bound to dGTP (2'-deoxyguanosine 5'-triphosphate) and GTP (guanosine 5'-triphosphate). Native mass spectra for oncogenic mutants acquired with the same instrument settings also show binding of dGDP, GDP, GTP, and dGTP (Figure S1 and Table S4). However, a peak with a molecular weight greater than the mass of GTP is also observed for K-RAS^{G13D} (Figure S1B). In addition, adducts, such as sodium and magnesium, are bound to K-RAS and its mutants (Figure S1D). There are also considerable differences in the mole fractions of dGDP, GDP, dGTP, and GTP bound to K-RAS and its oncogenic mutants (Figure 1C,D). For example, the wild-type (WT) protein has an almost equal abundance of dGTP and GTP bound, whereas K-RAS^{Q61H} and K-RAS^{G12C} were bound to a larger fraction of GTP and dGTP, respectively. These results illustrate the ability of native MS to provide insight into sample heterogeneity and also suggest that each oncogenic mutant may have different affinities for the 2'-deoxy versus 2'-hydroxy forms of guanosine nucleotides.

Collision Cross Section (CCS) Measurements of K-RAS and Its Oncogenic Mutants Bound to GTP. To structurally compare the active state of K-RAS with those of its oncogenic mutants, K-RAS proteins loaded with GTP were analyzed by ion mobility mass spectrometry. The native mass spectra show that the proteins are predominantly bound to GTP and adducts with a molecular weight consistent with sodium or magnesium (Figures S2 and S3). K-RAS-GTP bound to a single magnesium is the most abundant species for the GTP-bound enzyme. The previously bound adducts in the “as-isolated” samples are completely removed. The rotationally averaged CCS values of K-RAS and its mutants were measured

using an ion mobility mass spectrometer. Figure 2A shows the mass spectrum of K-RAS and its representative ion mobility mass spectrum. The ion mobility mass spectra for G13D and G12C and arrival time distributions (ATDs) for K-RAS-GTP and its mutants are shown in Figures S3 and S4.

The CCS values for K-RAS and its mutants bound to GTP are largely similar with the exception of that of K-RAS^{Q61H} (Figure 2B), which has a smaller CCS implying that the protein complex is more compact (Table 1). A slightly larger

Table 1. Collision Cross Section (CCS) Values for the 8+ Charge State of K-RAS and Its Mutants Bound to GTP^a

protein	CCS (Å ²)
K-RAS	1932.3 ± 1.1
K-RAS ^{G12C}	1937.7 ± 2.8
K-RAS ^{G13D}	1939.5 ± 1.3
K-RAS ^{Q61H}	1921.7 ± 2.9

^aReported are the mean and standard deviation for the centroid CCS values ($n = 3$).

CCS is measured for K-RAS^{G12C} and K-RAS^{G13D} compared to that of the WT, suggesting that substitution of glycine with either cysteine or aspartic acid may reorganize the conformation of the protein. No statistical difference was observed for the centroid CCS values determined for K-RAS and its mutants bound to dGTP (Table S5). The CCS values overall are in agreement with those calculated⁵⁶ for the crystal structures (Table S6).

Intrinsic GTPase Activity of K-RAS and Its Mutants.

To monitor the intrinsic GTPase activity, the molecular weights of K-RAS and its oncogenic mutants loaded with GTP were monitored over time using native mass spectrometry (Figure 3). At the start of the reaction, the proteins are predominantly loaded with GTP (Figure 3A and Figure S2). A number of adducts consistent with the molecular weight of magnesium or sodium are present, and these adducts were accounted for when deconvoluting mass spectra. After incubation at 25 °C for 360 min, the hydrolysis of GTP to GDP and inorganic phosphate by K-RAS is evident by the loss of mass from K-RAS-GTP giving rise to a signal for K-RAS bound to GDP (Figure 3A). The theoretical monoisotopic

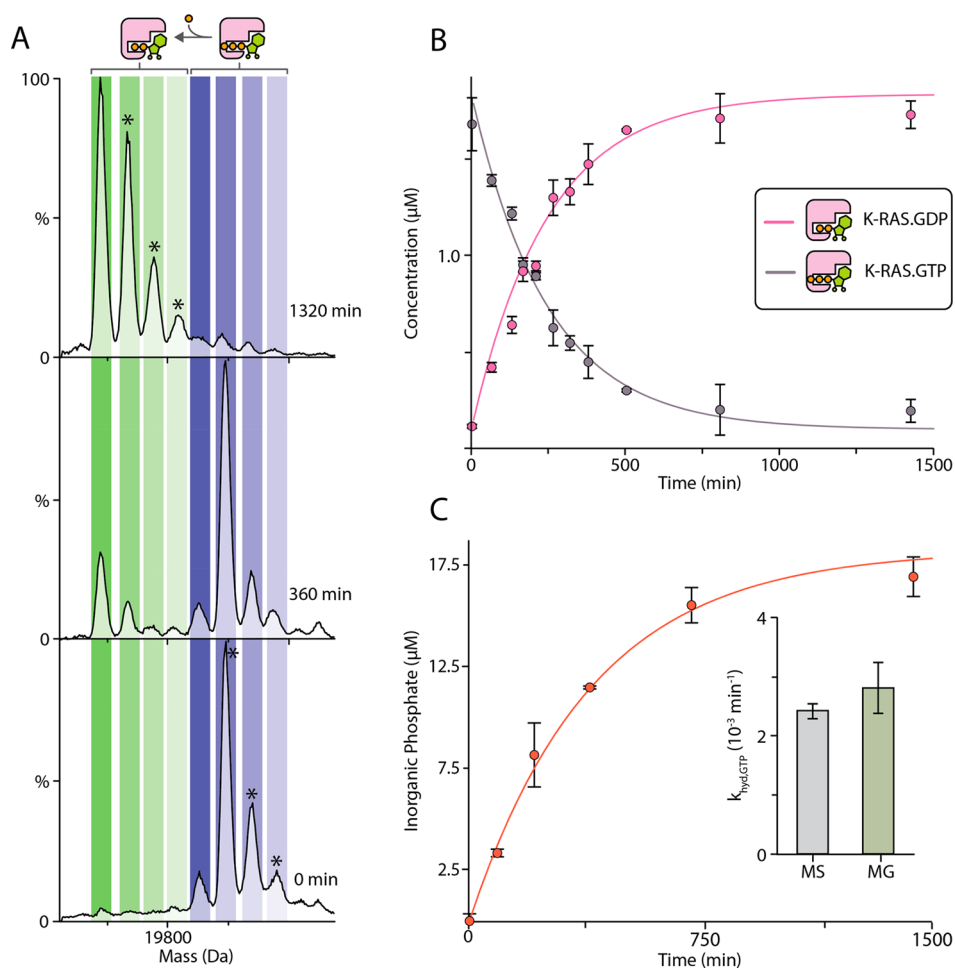


Figure 3. Determination of the GTP hydrolysis rate ($k_{\text{hyd,GTP}}$) for K-RAS. (A) Representative native mass spectra recorded at different time points for K-RAS (2 μM) loaded with GTP incubated at 25 °C. The abundance of K-RAS bound to GDP increases as GTP is hydrolyzed. Asterisks denote species with bound sodium or magnesium adducts. (B) The concentration of K-RAS bound to GDP and GTP was determined from deconvolution of native MS data (dots) and fit to a first-order rate constant model (solid lines) using KinTek Explorer Software.^{57,58} (C) Plot of inorganic phosphate concentration determined for K-RAS-GTP (20 μM) using a malachite green assay as a function of time (dots) and fit to a first-order rate constant model (solid lines). The inset shows the rate constants determined by native MS and a malachite green (MG) assay, which are statistically similar (two-tailed Student's t test; $p = 0.29$). Reported are the mean and standard deviation ($n = 3$).

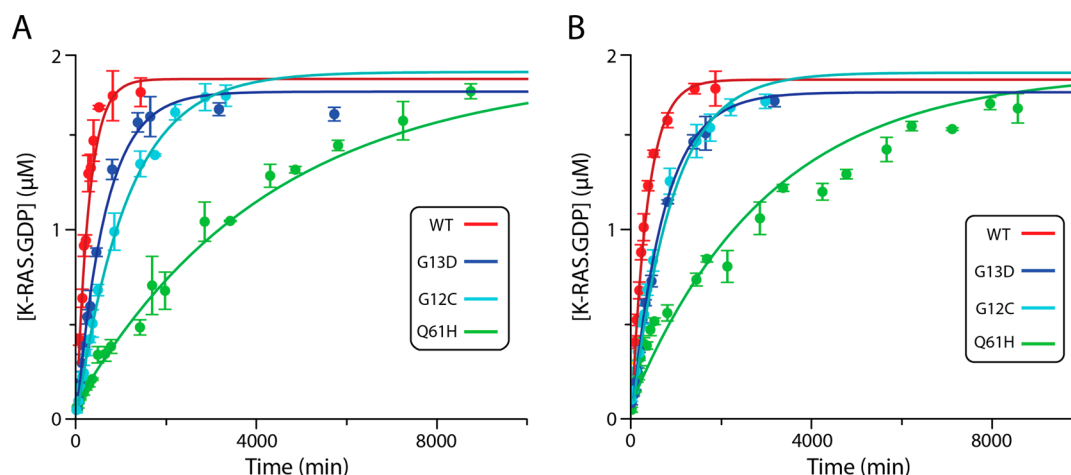


Figure 4. Kinetics of intrinsic GTPase activity for K-RAS and its mutants. Protein samples loaded with (A) GTP or (B) dGTP were incubated at 25 °C, and hydrolysis was monitored by native MS. Reported are the mean and standard deviation ($n = 3$).

mass for HPO_3^- is 80.0 Da, and the observed measured difference in mass as a result of hydrolysis is 80.9 Da. Notably, the loss of mass in K-RAS·GTP corresponds to HPO_3^- , but this leaves the enzyme as inorganic phosphate (PO_4^{2-}). The hydrolysis of GTP nearly reaches completion after 1260 min, and the predominate signal is for K-RAS bound to GDP. The concentrations of K-RAS bound to GDP and GTP, including the species adducted with magnesium or sodium, were determined from deconvolution of mass spectral data and fit to a first-order rate constant model using KinTek Explorer Software^{57,58} to determine the intrinsic rate of GTP hydrolysis ($k_{\text{hyd,GTP}}$) (Figure 3B). Figure 3B shows the fit of this model to the data. The $k_{\text{hyd,GTP}}$ for K-RAS at 25 °C in 200 mM ammonium acetate (pH 7.4) is $2.42 \times 10^{-3} \text{ min}^{-1}$.

To validate the $k_{\text{hyd,GTP}}$ value determined by native MS, an established solution assay was used to monitor the intrinsic GTPase activity of K-RAS.^{59,60} The concentration of inorganic phosphate was quantified over time for K-RAS loaded with GTP at 25 °C, and $k_{\text{hyd,GTP}}$ was determined as it was for the native MS data (Figure 3C). The $k_{\text{hyd,GTP}}$ values determined by the two techniques are statistically indistinguishable. These results corroborate the native MS-derived values and indicate that GDP remains bound to K-RAS after inorganic phosphate is released.

In a fashion similar to that for the WT protein, the intrinsic GTPase activity of K-RAS oncogenic mutants was determined by native MS. Again, the hydrolysis of GTP by K-RAS mutants is monitored directly by the appearance and disappearance of signals corresponding to the protein bound to GDP and GTP, respectively (Figure 4A).

In general, the $k_{\text{hyd,GTP}}$ values were lower for the oncogenic mutants that were studied than for the WT protein (Figure S5A and Table 2). K-RAS^{Q61H} has the smallest $k_{\text{hyd,GTP}}$ compared to those of the other mutants, nearly 10-fold lower than that of the WT protein. The mutant proteins have hydrolysis rates that are lower than that of the WT but differ among themselves.

Intrinsic Hydrolysis of dGTP by K-RAS and Its Oncogenic Mutants. Inspired by the observation of dGDP and dGTP bound to the “as-isolated” proteins, we loaded K-RAS and its mutants with dGTP and measured the intrinsic hydrolysis (Figure S6). For K-RAS, no statistically significant difference was observed for the rate of dGTP hydrolysis

Table 2. GTP and dGTP Intrinsic Hydrolysis Rates ($\times 10^{-3} \text{ min}^{-1}$) at 25 °C^a

protein	$k_{\text{hyd,GTP}} \pm$ standard deviation	$k_{\text{hyd,dGTP}} \pm$ standard deviation	$k_{\text{hyd,dGTP}}/k_{\text{hyd,GTP}} \pm$ relative uncertainty	p value
WT	2.42 ± 0.1	1.91 ± 0.52	0.79 ± 0.27	0.2409
G12C	0.68 ± 0.06	1.5 ± 0.11	2.20 ± 0.11	0.0008
G13D	0.92 ± 0.06	1.19 ± 0.03	1.29 ± 0.07	0.0044
Q61H	0.25 ± 0.01	0.38 ± 0.02	1.52 ± 0.06	0.0013

^aReported are the mean and standard deviation ($n = 3$) and the p value from the two-tailed Student's t test comparing $k_{\text{hyd,GTP}}$ and $k_{\text{hyd,dGTP}}$.

($k_{\text{hyd,dGTP}}$) compared to $k_{\text{hyd,GTP}}$ (Figure 4B, Figure S5B, and Table 2). In contrast, $k_{\text{hyd,dGTP}}$ values for K-RAS^{G12C}, K-RAS^{G13D}, and K-RAS^{Q61H} differed from the rates measured for GTP (Figure S5B and Table 2). Interestingly, the ratio of $k_{\text{hyd,dGTP}}$ to $k_{\text{hyd,GTP}}$ indicates that these three mutants (G12C, G13D, and Q61H) hydrolyze dGTP at a higher rate, more than 2-fold that for K-RAS^{G12C}. In other words, the half-lives for these three mutants are much longer for the enzyme bound to GTP compared to that for the enzyme bound to dGTP. These results indicate that these oncogenic mutants preferably hydrolyze the 2'-deoxy form of GTP.

Activation Energetics of Intrinsic GTPase Activity for K-RAS and Its Oncogenic Mutants. To determine the energetic barriers of intrinsic GTPase activity, the hydrolysis of GTP by K-RAS and mutants incubated at three additional temperatures (10, 30, and 37 °C) was monitored by native MS. The $k_{\text{hyd,GTP}}$ values were determined for the different temperatures, which increased with an increase in temperature (Figure 5 and Figure S7).

The $k_{\text{hyd,GTP}}$ values at different temperatures were used for Eyring analysis,⁵⁵ where the natural logarithm of $k_{\text{hyd,GTP}}$ divided by temperature is plotted against the reciprocal temperature (Figure S8). The data were fit to the Eyring equation to determine the transition state enthalpy (ΔH^\ddagger) and entropy (ΔS^\ddagger) (Table 3 and Figure S9). The thermodynamic parameters for K-RAS derived from Eyring analysis are as follows: $\Delta H^\ddagger = 17 \text{ kcal/mol}$, $T\Delta S^\ddagger = -3.9 \text{ kcal/mol}$ ($T = 298 \text{ K}$), and $\Delta G^\ddagger = 21 \text{ kcal/mol}$. For all proteins studied, the barrier of the transition state is dominated by a large positive ΔH^\ddagger and to lesser extent by a small unfavorable contribution

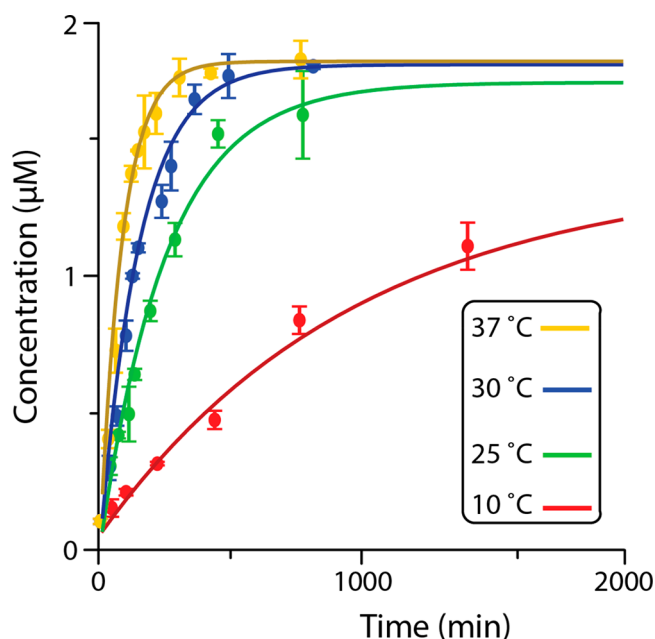


Figure 5. Temperature dependence of the intrinsic GTPase activity of K-RAS. Protein samples were incubated at four different temperatures (10, 25, 30, and 37 °C), and the intrinsic hydrolysis was monitored using native MS. Reported are the mean and standard deviation ($n = 3$).

from ΔS^\ddagger . Interestingly, the K-RAS oncogenic mutants have ΔH^\ddagger values larger than that of the WT, explaining the decrease in $k_{\text{hyd,GTP}}$ (Table 3). The $\Delta\Delta H^\ddagger$ ($\Delta H^\ddagger_{\text{mutant}} - \Delta H^\ddagger_{\text{WT}}$) depends on the mutant but ranges from 1.0 to 2.6 kcal/mol. In contrast, the ΔS^\ddagger term becomes more favorable for K-RAS^{G12C} and K-RAS^{Q61H}. Interestingly, the activation energetics for K-RAS^{G13D} was similar to that of the WT protein. Moreover, the activation energetics of K-RAS hydrolyzing dGTP is similar to that determined for the enzyme loaded with GTP (Figure S8B and Table S7).

DISCUSSION

Native Mass Spectra of K-RAS and Its Mutants. Native mass spectra of K-RAS and its mutants reveal heterogeneity in guanosine nucleotides bound to the enzyme. The data show binding of 2'-deoxy and 2'-hydroxy forms of GDP and GTP. Binding of 2'-deoxy guanosine nucleotides has been previously reported.²⁹ K-RAS and its mutants were expressed and purified from *E. coli*, where the concentration is 18-fold higher for GTP than for dGTP.⁶¹ Interestingly, the ratio of GDP to dGDP is 4 for K-RAS, considerably less than the ratio of the nucleotide pool in the expression host. While the abundances of the GTP- and dGTP-bound nucleotides are almost similar for K-RAS and K-RAS^{G13D}, K-RAS^{G12C} has more dGTP bound, implying that the affinity for this nucleotide might be higher. Another

interesting observation is the abundance of a bound adduct with a mass larger than that of GTP for K-RAS^{G13D} (Figure S1B). The observed adduct has a mass difference of approximately +133 Da from GDP, which is consistent with the mass of a ribosyl group. Because this adduct was not observed after loading K-RAS^{G13D} with GTP or dGTP, it indicates the molecule is bound noncovalently and does not have any effect on GTP hydrolysis. Identification of this ligand and its biological relevance for G13D function warrant further investigation. Native MS results reveal intrinsic differences in K-RAS and its variants, implying unique biochemical binding properties.

Ion Mobility Mass Spectrometry Measurements.

Native ion mobility measurements of K-RAS and its oncogenic mutants indicate that a native-like structure is preserved in the ion mobility mass spectrometer. An NMR study suggests that H-RAS bound to a nonhydrolyzable analogue of GTP (GppNHp) populates active and inactive conformations that interconvert on the millisecond time scale.^{62–64} Moreover, molecular dynamics simulations of oncogenic mutants, including G12D, G13D, and Q61H, suggest that these proteins mainly populate an active conformation, whereas G12C behaves like K-RAS populating two conformations.⁶⁵ The ATD for K-RAS and mutants did not exhibit mobility profiles with multiple peaks. The centroid CCS values are different for the WT and mutants. For example, the CCS values for K-RAS^{G12C} and K-RAS^{G13D} bound to GTP are larger than that of the WT (Figure S4A,C). The CCS for K-RAS^{Q61H} bound to GTP is smaller than those of the other proteins, indicating a more compact conformation that is also evident from the width of the ATD (Figure S4B and Table 1). From X-ray crystallography studies, H61 of K-RAS^{Q61H} is less exposed to the solvent due to formation of a hydrophobic cluster above the complex of the nucleotide and water.⁶⁶ This is consistent with the smaller CCS measured for this oncogenic mutant. These results show that native IM-MS can be informative for structural changes induced by mutation, and the development of higher-resolution IM-MS instruments^{67,68} has great potential to capture different conformations of K-RAS that have been observed by NMR and X-ray crystallography.

Monitoring GTPase Activity by High-Resolution

Native MS. As revealed by high-resolution native mass spectra, both 2'-deoxy and 2'-hydroxy forms of guanosine nucleotides were bound in the “as-isolated” samples, prompting us to determine the intrinsic dGTPase activity. Several factors can impact the rate of hydrolysis, including the temperature, buffer, ionic strength, pH, and concentration of divalent metal ion, magnesium.⁶⁹ The intrinsic GTP hydrolysis activity for K-RAS is consistent with other reports using NMR and radioactive methods.^{20,70} Moreover, MS-derived rates are in direct agreement with those determined by a solution-based assay.

Table 3. Transition State Thermodynamics for the Intrinsic GTPase Activity of K-RAS and Its Oncogenic Mutants^a

protein	ΔH^\ddagger (kcal/mol)	ΔS^\ddagger (kcal/mol)	ΔG^\ddagger (kcal/mol)	$\Delta\Delta S^\ddagger$ (kcal/mol)	$\Delta\Delta H^\ddagger$ (kcal/mol)
WT	17.0 ± 0.3	−0.0133 ± 0.0011	20.9 ± 0.01		
G12C	19.3 ± 0.1	−0.0084 ± 0.0005	21.8 ± 0.01	0.0049 ± 0.0012	2.3 ± 0.4
G13D	18.0 ± 0.5	−0.0119 ± 0.0018	21.6 ± 0.02	0.0014 ± 0.0021	1.0 ± 0.6
Q61H	19.6 ± 0.5	−0.0076 ± 0.0014	22.3 ± 0.02	0.0058 ± 0.0018	2.6 ± 0.6

^a ΔG^\ddagger is calculated directly from enthalpy and entropy at 25 °C. Reported are the mean and standard deviation of three replicates ($n = 3$).

The intrinsic GTPase activity for oncogenic mutants reveals differences in hydrolysis rates of dGTP compared to those of GTP. However, no difference in hydrolysis rates of dGTP and GTP was observed for K-RAS. For K-RAS^{Q61H}, K-RAS^{G12C}, and K-RAS^{G13D}, the rate of dGTP hydrolysis was higher than that for GTP. From atomic structures of K-RAS and its mutants, the ribose of the bound nucleotide is in a 2'-endo conformation, and the 2'-hydroxyl group forms weak hydrogen bonds with the side chain of Asp30 and the carbonyl group of Val29.⁷¹ When dGTP is replaced with GTP, these hydrogen bonds are lost, which probably leads to reordering of the nucleotide and subsequently the enhancement of enzyme activity.

RAS oncogenes have the ability to reprogram the metabolic process in cancer cells.⁷² It has also been established that imbalances in the deoxyribonucleotide triphosphate (dNTP) pool are directly associated with different diseases, including diabetes, obesity, and cancer, due to enhanced mutagenesis that causes genomic instability.⁷³ The relationship of the dNTP pool and our observation of higher dGTP intrinsic hydrolysis rates for oncogenic mutants compared to that of the WT protein warrant further investigation.

Activation Energetics of Intrinsic GTPase Activity.

Activation energetics was determined for the intrinsic GTPase activity of K-RAS and its mutants, providing insight into the barriers of the transition state. The values determined for GTPase activity of K-RAS are in excellent agreement with FT-IR data³³ ($\Delta H^\ddagger = 19.8$ kcal/mol, and $T\Delta S^\ddagger = -2.3$ kcal/mol) and molecular dynamics (MD) simulations ($\Delta H^\ddagger = 17.4$ kcal/mol, and $T\Delta S^\ddagger = -4$ kcal/mol).⁷⁴ The observed small entropic effects of K-RAS-catalyzed hydrolysis of GTP are consistent with MD simulations that showed $\Delta\Delta S^\ddagger$ ($\Delta S^\ddagger_{\text{enzyme}} - \Delta S^\ddagger_{\text{water}}$) makes a small contribution to the catalysis because reactants do not lose their entire translational and rotational motion when they are bound to the enzyme.⁷⁵ The large enthalpic barrier is also consistent with studies by Warshel et al. that showed less free energy needed to orient dipoles at the active site of an enzyme compared to uncatalyzed reactions in water because the active site of the protein includes the ionized residues, polar groups, and water molecules.⁷⁶ This highly polar and reorganized active site of the enzyme suggests that the enthalpic effects make more contributions in catalysis, and the small reorganization energy is paid during enzyme folding.^{75,77} There is an increase in enthalpy for all of the oncogenic mutants studied ($\Delta\Delta H^\ddagger$) and a small increase in entropy ($\Delta\Delta S^\ddagger$) for the transition state of intrinsic GTPase activity. The value for $\Delta\Delta H^\ddagger$ is higher for K-RAS^{Q61H}, explaining why the hydrolysis rate for this mutant is much slower followed by K-RAS^{G12C} and K-RAS^{G13D}. The activation energetics for K-RAS and its oncogenic mutants explains their different rates of GTP hydrolysis.

In summary, high-resolution native MS was used to determine the kinetics and thermodynamics of intrinsic GTP hydrolysis of K-RAS and its mutants. Native MS is a rapid and sensitive (minimal sample consumption) technique that revealed heterogeneity of the nucleotide bound to the "as-isolated" proteins. For oncogenic mutants, the rates of hydrolysis of dGTP were faster than those of GTP hydrolysis. This result implies that the mutants bound to dGTP spend less time in an active state. Moreover, activation energetics reveals the barrier of the transition state is dominated by enthalpy and to a much lesser extent by entropy. The decrease in the level of

intrinsic hydrolysis for oncogenic mutants is due to an increase in the enthalpic barrier.

■ ASSOCIATED CONTENT

Supporting Information

The Supporting Information is available free of charge on the ACS Publications website at DOI: 10.1021/acs.biochem.9b00532.

Deconvoluted mass spectra for K-RAS and its mutants, ion mobility mass spectra for K-RAS^{G12C} and K-RAS^{G13D}, ATD plots for K-RAS and its mutants, temperature dependence of rate constants and Eyring plots, optimized parameters for IM-MS analysis, and additional figures and tables (PDF)

■ AUTHOR INFORMATION

Corresponding Author

*E-mail: ALaganowsky@chem.tamu.edu.

ORCID

David E. Clemmer: 0000-0003-4039-1360

Arthur Laganowsky: 0000-0001-5012-5547

Funding

This work is supported by National Institutes of Health (NIH) via grants from the National Cancer Institute and the National Institute of General Medical Sciences awarded to D.E.C., D.H.R., and A.L. (RO1GM121751) and NIH Grant P41GM128577.

Notes

The authors declare no competing financial interest.

■ ACKNOWLEDGMENTS

The authors thank Dr. Thomas Meek (Texas A&M University) for useful discussion.

■ ABBREVIATIONS

dGDP, 2'-deoxyguanosine 5'-diphosphate; dGTP, 2'-deoxyguanosine 5'-triphosphate; IM-MS, ion mobility mass spectrometry; CCS, collision cross section; ATD, arrival time distribution.

■ REFERENCES

- (1) Wiesmuller, L., and Wittinghofer, F. (1994) Signal-Transduction Pathways Involving Ras. *Cell. Signalling* 6, 247–267.
- (2) Pylayeva-Gupta, Y., Grabocka, E., and Bar-Sagi, D. (2011) RAS oncogenes: weaving a tumorigenic web. *Nat. Rev. Cancer* 11, 761–774.
- (3) Drosten, M., Dhawahir, A., Sum, E. Y. M., Urosecic, J., Lechuga, C. G., Esteban, L. M., Castellano, E., Guerra, C., Santos, E., and Barbacid, M. (2010) Genetic analysis of Ras signalling pathways in cell proliferation, migration and survival. *EMBO J.* 29, 1091–1104.
- (4) Downward, J. (2003) Targeting RAS signalling pathways in cancer therapy. *Nat. Rev. Cancer* 3, 11–22.
- (5) Colicelli, J. (2004) Human RAS superfamily proteins and related GTPases. *Sci. Signaling* 2004, RE13.
- (6) Goitre, L., Trapani, E., Trabalzini, L., and Retta, S. F. (2014) The Ras superfamily of small GTPases: the unlocked secrets. *Methods Mol. Biol.* 1120, 1–18.
- (7) Bourne, H. R., Sanders, D. A., and McCormick, F. (1991) The GTPase superfamily: conserved structure and molecular mechanism. *Nature* 349, 117–127.
- (8) Downward, J. (1990) The ras superfamily of small GTP-binding proteins. *Trends Biochem. Sci.* 15, 469–472.

- (9) Vetter, I. R., and Wittinghofer, A. (2001) The Guanine Nucleotide-Binding Switch in Three Dimensions. *Science* 294, 1299–1304.
- (10) Wennerberg, K., Rossman, K. L., and Der, C. J. (2005) The Ras superfamily at a glance. *J. Cell Sci.* 118, 843–846.
- (11) Lu, S., Jang, H., Muratcioglu, S., Gursoy, A., Keskin, O., Nussinov, R., and Zhang, J. (2016) Ras Conformational Ensembles, Allostery, and Signaling. *Chem. Rev.* 116, 6607–6665.
- (12) Vetter, I. R., and Wittinghofer, A. (2001) The guanine nucleotide-binding switch in three dimensions. *Science* 294, 1299–1304.
- (13) Cox, A. D., Fesik, S. W., Kimmelman, A. C., Luo, J., and Der, C. J. (2014) Drugging the undruggable RAS: Mission possible? *Nat. Rev. Drug Discovery* 13, 828–851.
- (14) Cherfils, J., and Zeghouf, M. (2013) Regulation of Small GTPases by GEFs, GAPs, and GDIs. *Physiol. Rev.* 93, 269–309.
- (15) Cox, A. D., and Der, C. J. (2010) Ras history: The saga continues. *Small GTPases* 1, 2–27.
- (16) Malumbres, M., and Barbacid, M. (2003) RAS oncogenes: the first 30 years. *Nat. Rev. Cancer* 3, 459–465.
- (17) Prior, I. A., Lewis, P. D., and Mattos, C. (2012) A comprehensive survey of Ras mutations in cancer. *Cancer Res.* 72, 2457–2467.
- (18) Forbes, S. A., Bindal, N., Bamford, S., Cole, C., Kok, C. Y., Beare, D., Jia, M., Shepherd, R., Leung, K., Menzies, A., Teague, J. W., Campbell, P. J., Stratton, M. R., and Futreal, P. A. (2011) COSMIC: mining complete cancer genomes in the Catalogue of Somatic Mutations in Cancer. *Nucleic Acids Res.* 39, D945–D950.
- (19) Miller, M. S., and Miller, L. D. (2012) RAS Mutations and Oncogenesis: Not all RAS Mutations are Created Equally. *Front. Genet.* 2, 100.
- (20) Smith, M. J., Neel, B. G., and Ikura, M. (2013) NMR-based functional profiling of RASopathies and oncogenic RAS mutations. *Proc. Natl. Acad. Sci. U. S. A.* 110, 4574–4579.
- (21) Schubert, S., Shannon, K., and Bollag, G. (2007) Hyperactive Ras in developmental disorders and cancer. *Nat. Rev. Cancer* 7, 295–308.
- (22) Vigil, D., Cherfils, J., Rossman, K. L., and Der, C. J. (2010) Ras superfamily GEFs and GAPs: validated and tractable targets for cancer therapy? *Nat. Rev. Cancer* 10, 842–857.
- (23) Fernandez-Medarde, A., and Santos, E. (2011) Ras in cancer and developmental diseases. *Genes Cancer* 2, 344–358.
- (24) Stephen, A. G., Esposito, D., Bagni, R. K., and McCormick, F. (2014) Dragging ras back in the ring. *Cancer Cell* 25, 272–281.
- (25) Karnoub, A. E., and Weinberg, R. A. (2008) Ras oncogenes: split personalities. *Nat. Rev. Mol. Cell Biol.* 9, 517–531.
- (26) Morelli, M. P., and Kopetz, S. (2012) Hurdles and Complexities of Codon 13 KRAS Mutations. *J. Clin. Oncol.* 30, 3565–3567.
- (27) Guerrero, I., Casanova, I., Farré, L., Mazo, A., Capellà, G., and Mangués, R. (2000) K-ras codon 12 mutation induces higher level of resistance to apoptosis and predisposition to anchorage-independent growth than codon 13 mutation or proto-oncogene overexpression. *Cancer Res.* 60, 6750–6756.
- (28) Kraus, M. C., Seelig, M. H., Linnemann, U., and Berger, M. R. (2006) The balanced induction of K-ras codon 12 and 13 mutations in mucosa differs from their ratio in neoplastic tissues. *Int. J. Oncol.* 29, 957–964.
- (29) Neal, S. E., Eccleston, J. F., Hall, A., and Webb, M. R. (1988) Kinetic analysis of the hydrolysis of GTP by p21N-ras. The basal GTPase mechanism. *J. Biol. Chem.* 263, 19718–19722.
- (30) Self, A. J., and Hall, A. (1995) [8] Measurement of intrinsic nucleotide exchange and GTP hydrolysis rates. In *Methods in Enzymology*, pp 67–76, Academic Press.
- (31) Webb, M. R., and Hunter, J. L. (1992) Interaction of GTPase-activating protein with p21ras, measured using a continuous assay for inorganic phosphate release. *Biochem. J.* 287 (Part 2), 555–559.
- (32) Gideon, P., John, J., Frech, M., Lautwein, A., Clark, R., Scheffler, J. E., and Wittinghofer, A. (1992) Mutational and kinetic analyses of the GTPase-activating protein (GAP)-p21 interaction: the C-terminal domain of GAP is not sufficient for full activity. *Mol. Cell. Biol.* 12, 2050–2056.
- (33) Kötting, C., and Gerwert, K. (2004) Time-resolved FTIR studies provide activation free energy, activation enthalpy and activation entropy for GTPase reactions. *Chem. Phys.* 307, 227–232.
- (34) Heck, A. J. R., and van den Heuvel, R. H. H. (2004) Investigation of intact protein complexes by mass spectrometry. *Mass Spectrom. Rev.* 23, 368–389.
- (35) Hilton, G. R., and Benesch, J. L. P. (2012) Two decades of studying non-covalent biomolecular assemblies by means of electrospray ionization mass spectrometry. *J. R. Soc., Interface* 9, 801–816.
- (36) Benesch, J. L. P., Ruotolo, B. T., Simmons, D. A., and Robinson, C. V. (2007) Protein Complexes in the Gas Phase: Technology for Structural Genomics and Proteomics. *Chem. Rev.* 107, 3544–3567.
- (37) Pacholarz, K. J., Garlish, R. A., Taylor, R. J., and Barran, P. E. (2012) Mass spectrometry based tools to investigate protein-ligand interactions for drug discovery. *Chem. Soc. Rev.* 41, 4335–4355.
- (38) Hilton, G. R., and Benesch, J. L. (2012) Two decades of studying non-covalent biomolecular assemblies by means of electrospray ionization mass spectrometry. *J. R. Soc., Interface* 9, 801–816.
- (39) Ruotolo, B. T., Giles, K., Campuzano, I., Sandercock, A. M., Bateman, R. H., and Robinson, C. V. (2005) Evidence for macromolecular protein rings in the absence of bulk water. *Science* 310, 1658–1661.
- (40) Ruotolo, B. T., Tate, C. C., and Russell, D. H. (2004) Ion mobility-mass spectrometry applied to cyclic peptide analysis: conformational preferences of gramicidin S and linear analogs in the gas phase. *J. Am. Soc. Mass Spectrom.* 15, 870–878.
- (41) Daneshfar, R., Kitova, E. N., and Klassen, J. S. (2004) Determination of protein-ligand association thermochemistry using variable-temperature nano-electrospray mass spectrometry. *J. Am. Chem. Soc.* 126, 4786–4787.
- (42) Rose, R. J., Damoc, E., Denisov, E., Makarov, A., and Heck, A. J. R. (2012) High-sensitivity Orbitrap mass analysis of intact macromolecular assemblies. *Nat. Methods* 9, 1084–1086.
- (43) Cong, X., Liu, Y., Liu, W., Liang, X., Russell, D. H., and Laganowsky, A. (2016) Determining Membrane Protein–Lipid Binding Thermodynamics Using Native Mass Spectrometry. *J. Am. Chem. Soc.* 138, 4346–4349.
- (44) Patrick, J. W., Boone, C. D., Liu, W., Conover, G. M., Liu, Y., Cong, X., and Laganowsky, A. (2018) Allostery revealed within lipid binding events to membrane proteins. *Proc. Natl. Acad. Sci. U. S. A.* 115, 2976–2981.
- (45) Shirzadeh, M., Boone, C. D., Laganowsky, A., and Russell, D. H. (2019) Topological Analysis of Transthyretin Disassembly Mechanism: Surface-Induced Dissociation Reveals Hidden Reaction Pathways. *Anal. Chem.* 91, 2345–2351.
- (46) Maple, H. J., Scheibner, O., Baumert, M., Allen, M., Taylor, R. J., Garlish, R. A., Bromirski, M., and Burnley, R. J. (2014) Application of the Exactive Plus EMR for automated protein-ligand screening by non-covalent mass spectrometry. *Rapid Commun. Mass Spectrom.* 28, 1561–1568.
- (47) Poltash, M. L., Shirzadeh, M., McCabe, J. W., Moghadamchagari, Z., Laganowsky, A., and Russell, D. H. (2019) New insights into the metal-induced oxidative degradation pathways of transthyretin. *Chem. Commun.* 55, 4091–4094.
- (48) Lanucara, F., Holman, S. W., Gray, C. J., and Eyers, C. E. (2014) The power of ion mobility-mass spectrometry for structural characterization and the study of conformational dynamics. *Nature. Nat. Chem.* 6, 281–294.
- (49) Laganowsky, A., Reading, E., Hopper, J. T., and Robinson, C. V. (2013) Mass spectrometry of intact membrane protein complexes. *Nat. Protoc.* 8, 639–651.
- (50) Marty, M. T., Baldwin, A. J., Marklund, E. G., Hochberg, G. K., Benesch, J. L., and Robinson, C. V. (2015) Bayesian deconvolution of mass and ion mobility spectra: from binary interactions to polydisperse ensembles. *Anal. Chem.* 87, 4370–4376.

- (51) May, J. C., Goodwin, C. R., Lareau, N. M., Leapfrog, K. L., Morris, C. B., Kurulugama, R. T., Mordehai, A., Klein, C., Barry, W., Darland, E., Overney, G., Imatani, K., Stafford, G. C., Fjeldsted, J. C., and McLean, J. A. (2014) Conformational Ordering of Biomolecules in the Gas Phase: Nitrogen Collision Cross Sections Measured on a Prototype High Resolution Drift Tube Ion Mobility-Mass Spectrometer. *Anal. Chem.* 86, 2107–2116.
- (52) Stow, S. M., Causon, T. J., Zheng, X., Kurulugama, R. T., Mairinger, T., May, J. C., Rennie, E. E., Baker, E. S., Smith, R. D., McLean, J. A., Hann, S., and Fjeldsted, J. C. (2017) An Interlaboratory Evaluation of Drift Tube Ion Mobility–Mass Spectrometry Collision Cross Section Measurements. *Anal. Chem.* 89, 9048–9055.
- (53) Lanzetta, P. A., Alvarez, L. J., Reinach, P. S., and Candia, O. A. (1979) An improved assay for nanomole amounts of inorganic phosphate. *Anal. Biochem.* 100, 95–97.
- (54) Quan, A., and Robinson, P. J. (2005) Rapid Purification of Native Dynamin I and Colorimetric GTPase Assay. In *Methods in Enzymology*, pp 556–569, Academic Press.
- (55) Eyring, H. (1935) The Activated Complex in Chemical Reactions. *J. Chem. Phys.* 3, 107–115.
- (56) Marklund, E. G., Degiacomi, M. T., Robinson, C. V., Baldwin, A. J., and Benesch, J. L. (2015) Collision cross sections for structural proteomics. *Structure* 23, 791–799.
- (57) Johnson, K. A., Simpson, Z. B., and Blom, T. (2009) Global kinetic explorer: a new computer program for dynamic simulation and fitting of kinetic data. *Anal. Biochem.* 387, 20–29.
- (58) Johnson, K. A., Simpson, Z. B., and Blom, T. (2009) FitSpace explorer: an algorithm to evaluate multidimensional parameter space in fitting kinetic data. *Anal. Biochem.* 387, 30–41.
- (59) Novelli, E. T., First, J. T., and Webb, L. J. (2018) Quantitative Measurement of Intrinsic GTP Hydrolysis for Carcinogenic Glutamine 61 Mutants in H-Ras. *Biochemistry* 57, 6356–6366.
- (60) Guymer, D., Maillard, J., Agacan, M. F., Brearley, C. A., and Sargent, F. (2010) Intrinsic GTPase activity of a bacterial twin-arginine translocation proofreading chaperone induced by domain swapping. *FEBS J.* 277, 511–525.
- (61) Buckstein, M. H., He, J., and Rubin, H. (2008) Characterization of Nucleotide Pools as a Function of Physiological State in *Escherichia coli*. *J. Bacteriol.* 190, 718–726.
- (62) Liao, J., Shima, F., Araki, M., Ye, M., Muraoka, S., Sugimoto, T., Kawamura, M., Yamamoto, N., Tamura, A., and Kataoka, T. (2008) Two conformational states of Ras GTPase exhibit differential GTP-binding kinetics. *Biochem. Biophys. Res. Commun.* 369, 327–332.
- (63) Shima, F., Ijiri, Y., Muraoka, S., Liao, J., Ye, M., Araki, M., Matsumoto, K., Yamamoto, N., Sugimoto, T., Yoshikawa, Y., Kumasaka, T., Yamamoto, M., Tamura, A., and Kataoka, T. (2010) Structural Basis for Conformational Dynamics of GTP-bound Ras Protein. *J. Biol. Chem.* 285, 22696–22705.
- (64) Araki, M., Shima, F., Yoshikawa, Y., Muraoka, S., Ijiri, Y., Nagahara, Y., Shirono, T., Kataoka, T., and Tamura, A. (2011) Solution Structure of the State 1 Conformer of GTP-bound H-Ras Protein and Distinct Dynamic Properties between the State 1 and State 2 Conformers. *J. Biol. Chem.* 286, 39644–39653.
- (65) Lu, S., Jang, H., Nussinov, R., and Zhang, J. (2016) The Structural Basis of Oncogenic Mutations G12, G13 and Q61 in Small GTPase K-Ras4B. *Sci. Rep.* 6, 21949.
- (66) Buhrman, G., Wink, G., and Mattos, C. (2007) Transformation Efficiency of RasQ61 Mutants Linked to Structural Features of the Switch Regions in the Presence of Raf. *Structure* 15, 1618–1629.
- (67) Poltash, M. L., McCabe, J. W., Shirzadeh, M., Laganowsky, A., Clowers, B. H., and Russell, D. H. (2018) Fourier Transform-Ion Mobility-Orbitrap Mass Spectrometer: A Next-Generation Instrument for Native Mass Spectrometry. *Anal. Chem.* 90, 10472–10478.
- (68) Glaskin, R. S., Valentine, S. J., and Clemmer, D. E. (2010) A Scanning Frequency Mode for Ion Cyclotron Mobility Spectrometry. *Anal. Chem.* 82, 8266–8271.
- (69) MISTOU, M.-Y., COOL, R. H., and PARMEGGIANI, A. (1992) Effects of ions on the intrinsic activities of c-H-ras protein p21. *Eur. J. Biochem.* 204, 179–185.
- (70) Wey, M., Lee, J., Jeong, S. S., Kim, J., and Heo, J. (2013) Kinetic Mechanisms of Mutation-Dependent Harvey Ras Activation and Their Relevance for the Development of Costello Syndrome. *Biochemistry* 52, 8465–8479.
- (71) Pai, E. F., Krengel, U., Petsko, G. A., Goody, R. S., Kabsch, W., and Wittinghofer, A. (1990) Refined crystal structure of the triphosphate conformation of H-ras p21 at 1.35 Å resolution: implications for the mechanism of GTP hydrolysis. *EMBO J.* 9, 2351–2359.
- (72) Pavlova, N. N., and Thompson, C. B. (2016) The Emerging Hallmarks of Cancer Metabolism. *Cell Metab.* 23, 27–47.
- (73) Buj, R., and Aird, K. M. (2018) Deoxyribonucleotide Triphosphate Metabolism in Cancer and Metabolic Disease. *Front. Endocrinol.* 9, 177.
- (74) Åqvist, J., and Kamerlin, S. C. L. (2016) Conserved Motifs in Different Classes of GTPases Dictate their Specific Modes of Catalysis. *ACS Catal.* 6, 1737–1743.
- (75) Villà, J., Štrajbl, M., Glennon, T. M., Sham, Y. Y., Chu, Z. T., and Warshel, A. (2000) How important are entropic contributions to enzyme catalysis? *Proc. Natl. Acad. Sci. U. S. A.* 97, 11899–11904.
- (76) Warshel, A. (1998) Electrostatic Origin of the Catalytic Power of Enzymes and the Role of Preorganized Active Sites. *J. Biol. Chem.* 273, 27035–27038.
- (77) Cannon, W. R., and Benkovic, S. J. (1998) Solvation, Reorganization Energy, and Biological Catalysis. *J. Biol. Chem.* 273, 26257–26260.